Magyarhoni Földtani Társulat
Földtani Közlöny
Hungarian Geological Society

154/3, 365–381., Budapest, 2024

DOI: 10.23928/foldt.kozl.2024.154.3.365

Formation of peralkaline rhyolite in the East African Rift System: the role of assimilation – a tribute to the career of Csaba SZABÓ

MORORÓ, Emanuel A. A.[1], BERKESI, Márta[1,2], TSAY, Alexandra[3], GUZMICS, Tibor[1]*

[1]Eötvös Loránd University, Institute of Geography and Earth Sciences, Department of Petrology and Geochemistry, Lithosphere Fluid Research Lab, Budapest, Hungary
[2]MTA-EPSS Lendület FluidsByDepth Research Group, Sopron, Hungary
[3]University of Geneva, Department of Earth Sciences, Geneva, Switzerland
*Corresponding author. Email: tibor.guzmics@gmail.com

Az asszimiláció szerepe peralkáli riolitok kialakulásában a Kelet-afrikai-árokrendszerben – tisztelgés SZABÓ Csaba szakmai pályája előtt

Összefoglalás

Riftesedő geodinamikai környezetben előforduló peralkáli riolitok keletkezését általában a bazaltokból eredő frakcionációs kristályosodással magyarázzák. A peralkáli riolitok alkáli-gazdag és szilícium-dioxidban telítetlen magmás kőzetekkel való tér- és időbeli összefüggését azonban nem tárták fel kellőképpen. Jelen tanulmányban olyan peralkáli riolitos üvegösszetételeket mutatunk be, amelyeket jelenleg az egyetlen aktív, karbonatitlávát is produkáló Oldoinyo Lengai vulkánnál, illetve annak nagyobb rendszerét képező Kelet-afrikai-árokrendszerben azonosítottunk. A vizsgált mintákban a metamorf kvarc és oligoklász az Oldoinyo Lengai magmatizmusra nem jellemző ásványegyüttes. A magmás alapanyag összetétele (peralkáli riolitos üveg, alkáli-gazdag klinopiroxén és anortoklász) viszont egy peralkáli, SiO_2-telítetlen olvadék és egy SiO_2-ban gazdag falkőzet reakciójára utal. A nyomelemadatok – különös tekintettel a plagioklászban a negatív Eu-anomália hiánya – elvetik a bazaltból törénő frakcionációs kristályosodási modellt. Eredményeink azt mutatják, hogy a kezdeti olvadék egy peralkáli fonolit lehetett (58 wt% SiO_2, peralkalinitási index: 2,6), amely asszimilálta a SiO_2-ban gazdag kéregkőzetet, létrehozva a peralkáli riolitot. Tanulmányunkban összehasonlítjuk az Oldoinyo Lengai peralkáli riolitjait a Kelet-afrikai-árokrendszer mentén fellelhető más peralkáli kőzetekkel. A tanulmányozott asszimiláció feltételezésünk szerint számos kontinentális rift környezetben kialakulhatott, ahol a SiO_2-telítetlen alkáli magmatizmus SiO_2-gazdag mellékkőzettel lépett kölcsönhatásba.

Kulcsszavak: peralkáli riolit, Oldoinyo Lengai, asszimiláció, megoszlási együttható

Abstract

The origin of peralkaline rhyolites in rift settings is usually explained by prolonged crystal fractionation of basalts. However, the temporal and spatial association of peralkaline rhyolites to alkaline silica-undersaturated rocks has not been sufficiently explored. Here, we present peralkaline rhyolite glass compositions formed at a currently active carbonatite volcano (Oldoinyo Lengai), East African Rift System. The studied samples preserve mineral assemblage incompatible with Oldoinyo Lengai magmatism (presence of metamorphic quartz and oligoclase as relict crystals), while an igneous groundmass (peralkaline rhyolite glass, alkali-rich clinopyroxene and anorthoclase) presents evidence for the assimilation of a silica-rich rock by an alkali-rich silica-undersaturated melt. Trace element data reject the possibility that peralkaline rhyolites were formed by fractional crystallization of basalts, as the expected negative Eu anomaly from plagioclase fractionation is absent. The initial melt composition could be estimated as phonolitic (58 wt% SiO2, 2.6 peralkalinity index). We argue that the formation of peralkaline rhyolites at Oldoinyo Lengai occurred through assimilation of silica-rich crustal rocks by a silica-undersaturated magma. In addition, we compare peralkaline rhyolites from Oldoinyo Lengai to other peralkaline rocks from the East African Rift System. We propose that the above assimilation model may form in any continental rift where a silica-undersaturated alkaline magmatism interacts with silica-rich country rocks.

Keywords: peralkaline rhyolite, Oldoinyo Lengai, assimilation, partition coefficient

Introduction

Evolution of basaltic magmas leading to the formation of rhyolites is known to involve prolonged crystal fractionation (MACDONALD et al. 2012) as a main diving process. A common type of rhyolites occurring in rift settings and associated with silica-undersaturated magmatism is peralkaline rhyolites (LEMASURIER et al. 2003, WHITE et al. 2012). Several mechanisms have been proposed to explain their formation, including fractional crystallization of basaltic-basanitic magma (PECCERILLO et al. 2003, MACDONALD et al. 2008), partial melting of underplated basalts or continental crust followed by fractional crystallization (LOWENSTERN & MAHOOD 1991, TRUA et al. 1999), and assimilation of crustal rocks by basaltic magmas (MACDONALD et al. 2015). However, none of these mechanisms adequately explain the close association of silica-undersaturated rocks to highly peralkaline rhyolites (i.e., pantellerite). Phonolite/nephelinite compositions are not usually considered in rhyolite formation since the granite temperature minimum and the nepheline-syenite temperature minimum are separated by the alkali-feldspar thermal divide (KRACEK et al. 1937). Nevertheless, the formation of syenites from nepheline-normative melts through crustal contamination (JUNG et al. 2005) indicate that this thermal divide may be crossed in open systems where assimilation occurs. To explore how peralkaline silicate rocks relate to silica-undersaturated magmatism, we collected samples containing peralkaline rhyolite glass near the summit of a currently active carbonatite volcano (Oldoinyo Lengai) located in the East African Rift System. The collected samples were found enclosed in the nephelinite tuff in the form of volcanic bombs. We created a model explaining how peralkaline rhyolite can form through assimilation of a silica-rich rock by a silica-undersaturated melt. Additionally, we compare compositions generated through this process to other peralkaline rhyolites.

Geological background

East African Rift System

The East African Rift System (EARS) is a recently active continental extension zone (CHOROWICZ 2005, BRAILE et al. 2006) that hosts the highest density of silicic peralkaline volcanoes on Earth (CLARKE et al. 2019). It is traditionally divided into two main branches, Western and Eastern (*Fig. 1*), that split apart around the Tanzania Craton (CHOROWICZ 2005, BRAILE et al. 2006, DAWSON 2008). The Eastern branch (Gregory Rift) stretches from the Afar region through Ethiopia and Kenya to the North Tanzania Divergence (CHOROWICZ 2005, DAWSON 2008) and the Western branch extends from Lake Albert to Malawi (KAMPUNZU et al. 1998, CHOROWICZ 2005). The EARS can be further divided in several discrete and diachronous rift sectors: The Afar, Malawi, Rukwa, Tanganyika, Albert, Turkana and Gregory rifts (ROSENDAHL 1987, BRAILE et al. 2006). Rifting in the Afar region (Northern Ethiopia) has been interpreted as the first manifestation of extension of the EARS, at ~30 Ma (KELLER et al. 1994, CHOROWICZ 2005, DAWSON 2008). Volcanism began later in Northern Tanzania, at ~8 Ma (DAWSON 2008). At the northern part of the Western branch, volcanism started at ~12 Ma (KAMPUNZU et al. 1998). The EARS is still propagating southwards (CHOROWICZ 2005).

While leaving the cratonic areas mostly untouched, the EARS incises the circumcratonic metamorphic mobile belts surrounding the Tanzania Craton (MCCONNELL 1972, DAWSON 1992, KELLER et al. 1994, CHOROWICZ 2005). Both volcanic branches' orientations (western and eastern) follow the trace of earlier sutures (CHOROWICZ 2005). Crustal thickness along the rift axis varies from 20 km to 35 km, decreasing northwards (PRODEHL et al. 1994). Beneath the volcanic rift infills, the upper and middle crust is largely composed of Precambrian greenschist to amphibolite facies felsic-to-intermediate metamorphic rocks while the lower crust consists of granulite facies mafic rocks, mafic intrusions, and mafic rocks underplated onto the crust (MOONEY & CHRISTENSEN 1994).

Gregory Rift

Structures in the Gregory Rift mostly follow the N-S trend of the Mozambique belt (CHOROWICZ 2005, DAWSON 2008), which is composed of reworked Pre-Proterozoic and Neo-Proterozoic cratonic rocks and includes eclogites, gneisses, granitoids, granulite-gneisses together with younger metaigneous and metasedimentary rocks: gneisses, meta-anorthosites, enderbites, marbles and pegmatites (MUHONGO 1999, FRITZ et al. 2013).

The earliest erupted lavas in the Gregory Rift were mainly alkali basalts, trachytes and phonolites with smaller amounts of nephelinites, nepheline-phonolites and carbonatites (HAY et al. 1995, BRAILE et al. 2006, DAWSON 2008). Different varieties of plutonic rocks such as ijolites, syenites, nepheline-syenites, afrikandites, jacupiraguites, calciocarbonatites and pyroxenites also occur (DAWSON 1992, 2008; GUZMICS et al. 2012; KÁLDOS et al. 2015; HALÁSZ et al. 2023). The most prominent bimodal basalt-peralkaline silicic volcanic complexes located in the Gregory Rift (*Fig. 1*) are dominantly trachytic (Barrier, Emuruangogolak, Silali, Paka, Korosi, Menengai, Longonot, Suswa) or rhyolitic (Eburru, Olkaria), with basalts being volumetrically superior to intermediate rocks (SCAILLET & MACDONALD 2006, MACDONALD et al. 2008). The earliest peralkaline rhyolites occurring in the EARS formed approximately 32 Ma (HALDER et al. 2021). Along the Gregory Rift progressively younger formations (Eburru ~450 ka, Olkaria ~120 ka, Naivasha ~5 ka) occur southwards (*Fig. 1*; MACDONALD et al. 1987; MACDONALD & SCALIETT 2006; WHITE et al. 2012), matching the overall propagation of the EARS (CHOROWICZ 2005).

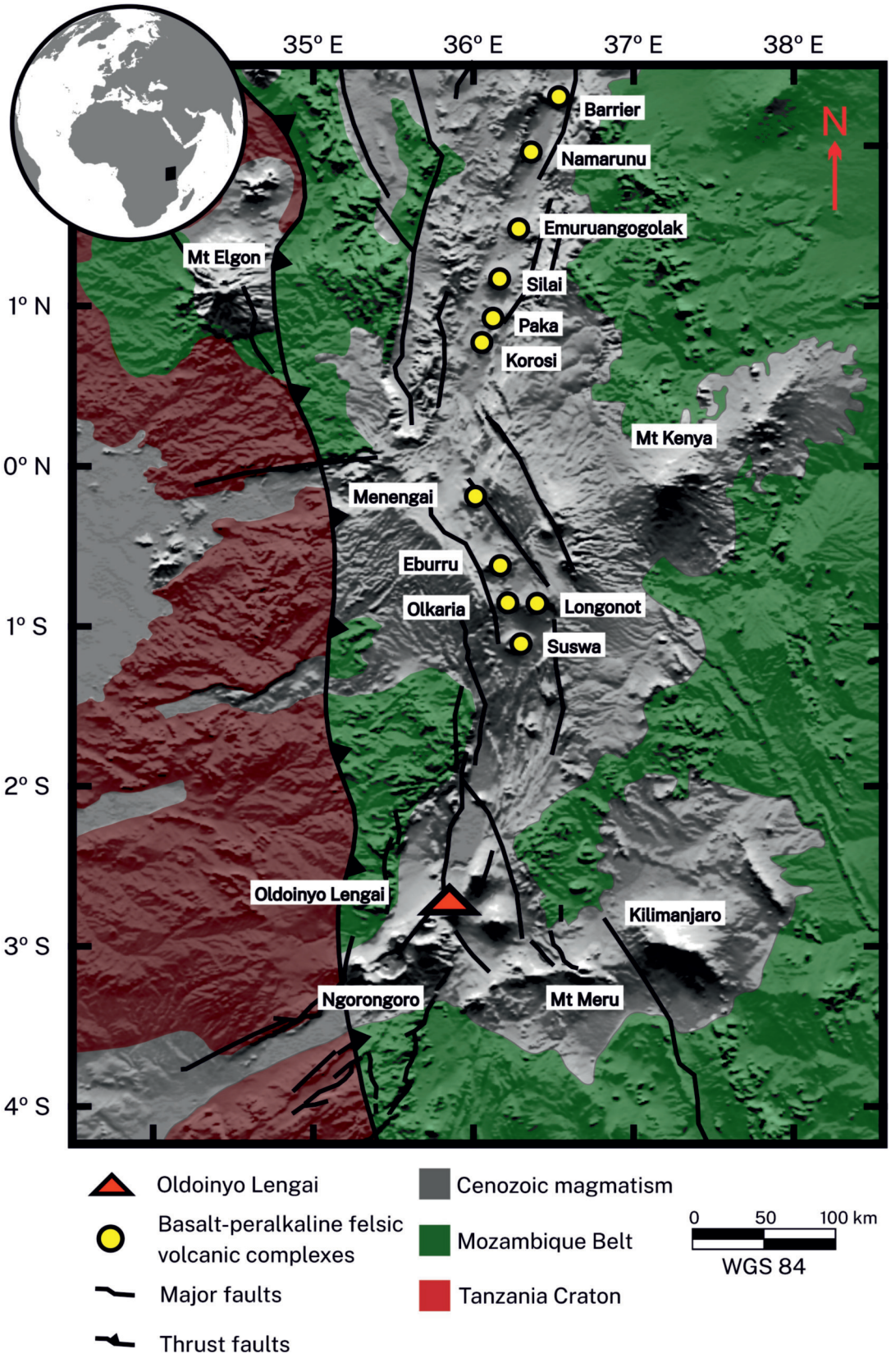

Figure 1. Location of Oldoinyo Lengai, basalt-peralkaline felsic volcanic complexes, Cenozoic magmatism, Mozambique belt, and Tanzania craton on the Gregory rift

1. ábra. *Az Oldoinyo Lengai vulkán, a bazalt-felzikus peralkáli vulkáni komplexumok, kainozoikumi magmatizmus, Mozambik-öv és Tanzánia-kraton elhelyezkedése a Gregory-rift térségében*

Material and Methods

Sampling and sample preparation

At the Oldoinyo Lengai volcano, located in the EARS (*Fig. 1*), characteristic rock samples (n = 5) were collected near the summit of the volcano (*Fig. 2A*). The studied samples occur as volcanic bombs within the combeite-wollastonite nephelinite tuff (*Fig. 2B*). Two double-polished thin sections (100 µm and 200 µm thick), representative of the collected set of samples, were prepared by sectioning the rock samples using a diamond saw. The desired thickness for the thin sections were obtained by lapping the sectioned rock slab on a glass plate, using 600 and 800 grit silicon carbide powder. Polishing was then performed using aluminum oxide abrasive powder on a cotton fabric. This procedure was done twice for each thin section. For petrographic study and to control the sample preparation steps a Nikon Eclipse LV100PL polarization microscope was used at the Lithosphere Fluid Research Lab, Eötvös University, Budapest (Hungary).

Scanning electron microscopy – Energy-dispersive X-ray spectroscopy (SEM-EDS)

SEM-EDS analysis was conducted on mineral and glass phases in thin sections to determine their major element compositions, using a Hitachi TM4000Plus microscope, in combination with a Quantax 75 EDS-SDD, at ELTE FS-RICF. Instrument settings were 15 kV accelerating voltage, 0.4 nA beam current and 15 seconds counting times, as efficient application was demonstrated by BERKESI et al. (2020). Low current conditions were used to minimize volatilization and consequent underestimation of Na. Cores and rims were analyzed in mineral phases that displayed compositional zoning. Cation number calculations for clinopyroxene were based on the assumption that the difference between cation numbers of ideal and measured compositions resulted from the presence of Fe^{3+} in the mineral structure. The Fe^{3+}/Fe^{2+} ratios were obtained through MS Office Excel 2019 iterative calculation function.

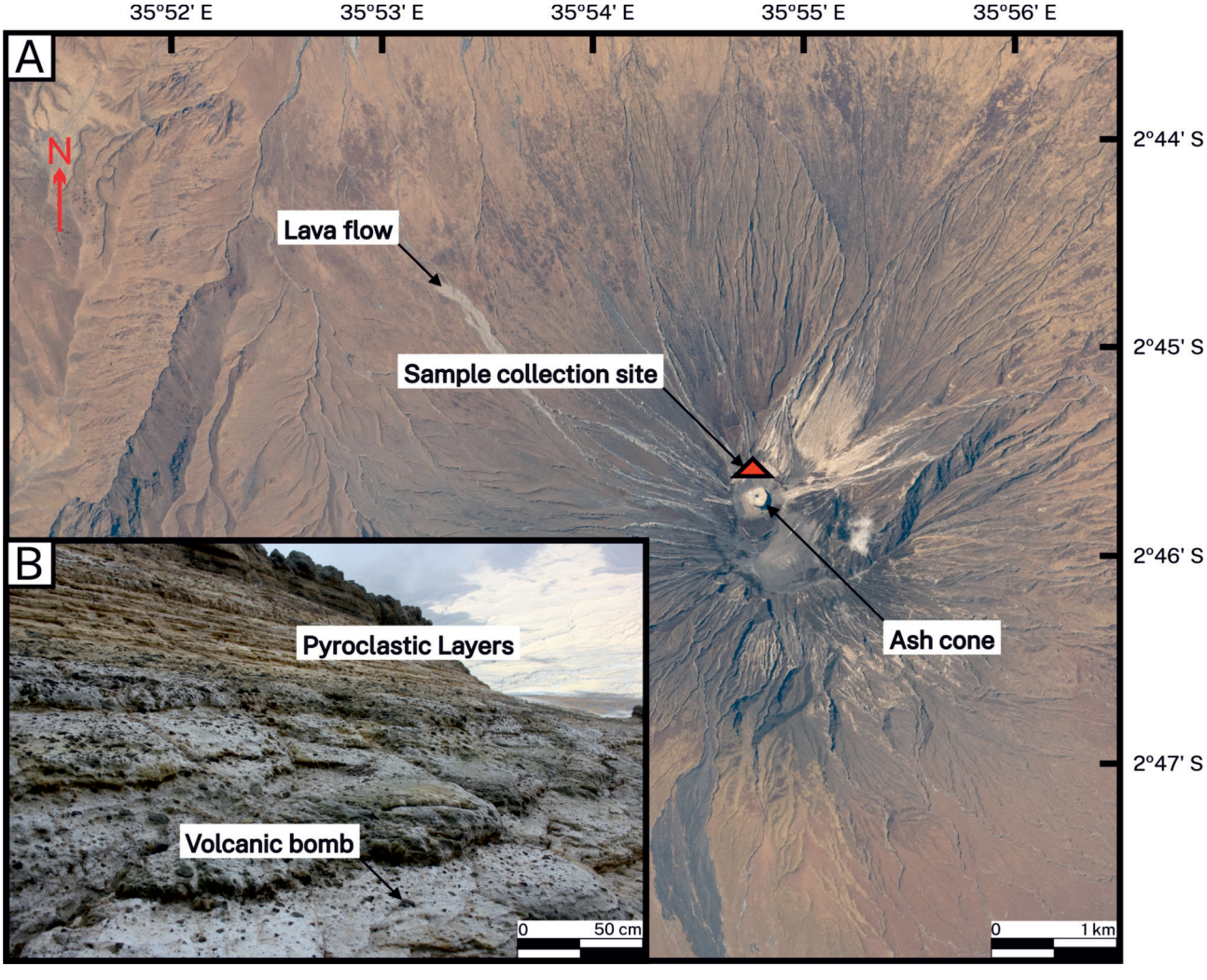

Figure 2. A) Spatial relations between the Oldoinyo Lengai summit and the sample collection site. B) Sample collection site, nephelinite tuff outcrop containing the studied volcanic bombs

2. ábra. *A) Az Oldoinyo Lengai csúcsa és a mintavételi hely közötti térbeli kapcsolat. B) Mintagyűjtő pont, amely egy nefelinittufa-réteg, és ahonnan a vizsgált vulkáni bombák előkerültek*

Laser Ablation – Inductively Coupled Plasma – Mass Spectrometry (LA-ICP-MS)

Mineral and glass phases were analyzed using an NWR 193 HE laser ablation system coupled with an Agilent 8900 triple-quadrupole mass spectrometer at the University of Geneva, Department of Earth Sciences. Samples were ablated with a He carrier gas flux of 0.82 to 0.87 L min^{-1}, pulse repetition rate of 8 Hz to 10 Hz, using spot sizes of 20 µm to 40 µm and laser fluence of 7.1 J cm^{-2}. NIST SRM610 and GSD-1G glasses were used as external standards. Data processing, utilizing SILLS software (GUILLONG et al. 2008), considered the total of major element oxides (SiO_2, TiO_2, Al_2O_3, Fe_2O_3, FeO, MnO, MgO, CaO, Na_2O, K_2O, and P_2O_5) equals to 100 wt%. Mineral and glass phases had the following isotopes measured with 10 milliseconds dwell time: ^{7}Li, ^{23}Na, ^{25}Mg, ^{27}Al, ^{29}Si, ^{31}P, ^{39}K, ^{43}Ca, ^{45}Sc, ^{49}Ti, ^{51}V, ^{52}Cr, ^{55}Mn, ^{56}Fe, ^{59}Co, ^{60}Ni, ^{65}Cu, ^{66}Zn, ^{85}Rb, ^{88}Sr, ^{89}Y, ^{90}Zr, ^{93}Nb, ^{95}Mo, ^{133}Cs, ^{137}Ba, ^{139}La, ^{140}Ce, ^{141}Pr, ^{146}Nd, ^{147}Sm, ^{153}Eu, ^{157}Gd, ^{159}Tb, ^{163}Dy, ^{165}Ho, ^{166}Er, ^{169}Tm, ^{172}Yb, ^{175}Lu, ^{178}Hf, ^{181}Ta, ^{182}W, ^{208}Pb, ^{232}Th, ^{238}U.

Results

Petrography

The studied samples are porphyritic xenoliths (*Fig. 3A*) consisting of two distinct parts: (1) large subparallel oriented quartz/feldspar (*Fig. 3B–C*) and (2) a fine-grained igneous groundmass. Quartz is colorless, subhedral, irregularly fractured, rounded, has no cleavage planes, shows undulatory extinction, and frequently presents dissolution features, with sizes ranging from 100 µm to 0.3 cm (*Fig. 3C*). Rutile needles and zircon occur as crystal inclusions hosted in quartz. Feldspar sizes range from 200 µm to 0.4 cm. The feldspar is grey to reddish grey, subhedral to anhedral, rounded, rarely twinned, frequently altered, and shows two cleavage planes. Feldspar crystals are zoned, with a 20 µm to 200 µm rim presenting distinct color and extinction angle (*Fig. 3C*). Secondary negative-crystal shaped to ellipsoidal fluid inclusions, varying in size from <1 µm to 50 µm, are abundant in quartz and feldspar cores (*Fig. 3D*) and are completely absent in groundmass crystals (*Fig. 3E*). Previous studies have shown an alkali-carbonate + sulfate + chloride-bearing, H_2O-poor, and CO_2-rich composition for these secondary quartz-hosted fluid inclusions at Oldoinyo Lengai (MORÓ et al. 2024).

Mineral phases in the groundmass are euhedral to subhedral titanite (30–150 µm), subhedral clinopyroxene (20–100 µm) and subhedral to anhedral groundmass feldspar (20–100 µm) (*Fig. 3E*). Titanite presents skeletal and poikilitic textures, containing clinopyroxene, feldspar and glass inclusions. Clinopyroxene is elongate with moderate green to yellow pleochroism, one observable cleavage plain and 3° to 5° extinction angle. Partial or complete replacement of feldspar by groundmass feldspar is observed throughout the sample. Interstitial glass is present between the crystals in the groundmass (*Fig. 3E*). Mineral modal proportions are the following: quartz ~15%, feldspar ~40%, ~10% clinopyroxene, ~25% groundmass feldspar, ~9% glass, ~1% titanite. Primary melt inclusions occur in groundmass crystals, albeit rarely, smaller inclusions contain only homogeneous glass while larger melt inclusions contain clinopyroxene and feldspar daughter crystals (*Fig. 3F*).

Mineral chemistry

SEM-EDS analyses showed that groundmass feldspar and the rims of feldspars are anorthoclase (*Fig. 4*) and have indistinct composition from each other, containing (all in mol%) 24.2–29.1 orthoclase ($KAlSi_3O_8$), 69.9–74.2 albite ($NaAlSi_3O_8$) and <1.6 anorthite ($CaAl_2Si_2O_8$) endmembers (*Table I, Supplementary Table I*). Relict feldspar cores are oligoclase (*Fig. 4*) and contain 4.3–5.5 orthoclase, 74.2–78.1 albite, 16.5–20.3 anorthite endmembers (*Table I, Supplementary Table I*). The clinopyroxenes show uniform aegirine-augitic composition (*Fig. 5*) being a solid solution of endmembers: 7.5–26.0 diopside ($CaMgSi_2O_6$), 13.5–26.7 hedenbergite ($CaFeSi_2O_6$), 42.6–58.6 aegirine ($NaFeSi_2O_6$), 1.8–13.9 titanian-aegirine ($Na(Fe,Ti)Si_2O_6$), <5.4% kosmochlor ($NaCrSi_2O_6$), <3.3% jadeite ($NaAlSi_2O_6$), <5.1% enstatite ($Mg_2Si_2O_6$), <0.3% wollastonite $Ca_2Si_2O_6$, <1.2% Ca-tschermak's $CaAlAlSiO_6$, <2.2% Fe-tschermak's ($CaFeAlSiO_6$) (*Table I, Supplementary Table II*). Titanite typically displays chemical zonation with Nb-rich cores (Nb_2O_5 > 1 wt%), and relatively Nb-poor outer rims (Nb_2O_5 0.1-0.9 wt% (*Table I, Supplementary Table III*). The glass is peralkaline rhyolitic in composition, (Na + K) / Al molar ratio (peralkalinity index) varies from 1.8 to 2.5, silica saturated, 70.6–73.4 wt% SiO_2, has a moderately-high Na_2O (5.8–7.8 wt%) and K_2O (4.4–5.1 wt%), Al_2O_3 content is low (6.9–7.9 wt%) (*Table I, Supplementary Table IV*). The glass found within homogeneous melt inclusions is also peralkaline rhyolitic in composition, presenting 66.01–67.66 wt% SiO_2, 7.73–10.49 wt% Na_2O, 4.85–5.96 wt% K_2O and 7.17–8.78 wt% Al_2O_3 (*Table I, Supplementary Table V*).

Trace element composition of constituents

LA-ICP-MS analyses showed that the titanite and peralkaline rhyolite glass were enriched in light REEs, relative to heavy REE based on chondrite-normalized patterns (*Fig. 6, Table II, Supplementary Table VI & VII*). Negative europium anomalies were not observed in groundmass crystals. High field strength elements (Th, U, Nb, Ta, Zr, Hf, W) are highly enriched in the peralkaline rhyolite glass. Rubidium, Sr and Eu are enriched while other large ion lithophile elements (Sr and Pb) present negative anomalies. Zinc is also marked by a strong negative anomaly.

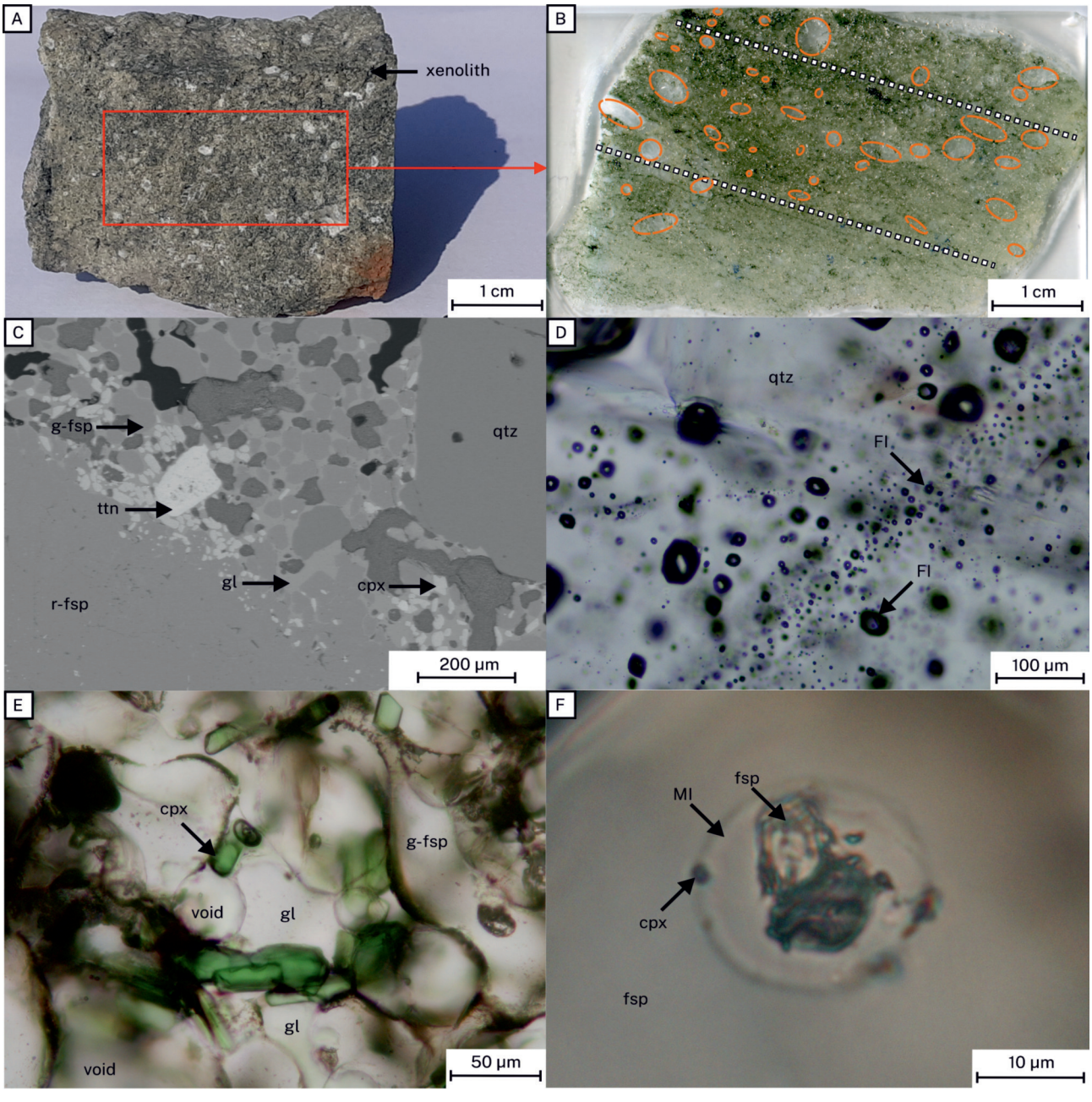

Figure 3. Photographs, photomicrographs, and backscattered electron images (BSE) showing the studied samples' characteristic petrographic features. A) Macroscopic appearance of a xenolith from Oldoinyo Lengai with highlighted outer tuffitic rim. B) Distribution of quartz and feldspar in a thin section (highlighted in orange). C) Details of groundmass phases (titanite, clinopyroxene, groundmass feldspar and glass) surrounding the feldspar (BSE image). D) Details of quartz-hosted fluid inclusions. E) Representative image of the groundmass. F) Detail of a groundmass feldspar-hosted melt inclusion containing feldspar and clinopyroxene daughter crystals

3. ábra. *Fényképek, mikroszkópos felvételek és visszaszórt elektronképek (BSE), amelyek a minták jellegzetes kőzettani jellemzőit mutatják. A) A bomba (xenolit) makroszkópos megjelenése a külső tufitos peremmel együtt. B) Kvarc és földpát mikroszkópos megjelenése (narancssárgával jelölve). C) A földpátot körülvevő alapanyag (titanit, klinopiroxén, földpát és kőzetüveg, visszaszórt elektronkép). D) A kvarcban lévő fluidumzárványok. E) Az alapanyag. F) Földpát- és klinopiroxén-leányásványokat tartalmazó, földpátba zárodott olvadékzárvány*

Discussion

Sample origin

The presence of oligoclase feldspar, quartz, and rhyolitic glass at Oldoinyo Lengai demands explanation, as Oldoinyo Lengai magmatism famously produces silica-undersaturated melts (KLAUDIUS & KELLER 2006, BERKESI et al. 2020).

Relict crystals

Compositional contrast between oligoclase feldspar and anorthoclase groundmass feldspar (*Fig. 4, Table I, Supplementary Table I*) excludes their formation from a common magmatic source. Anorthoclase groundmass feldspar is similar to feldspars found in peralkaline rhyolites at the EARS (*Fig. 4, Table I, Supplementary Table I*), while the

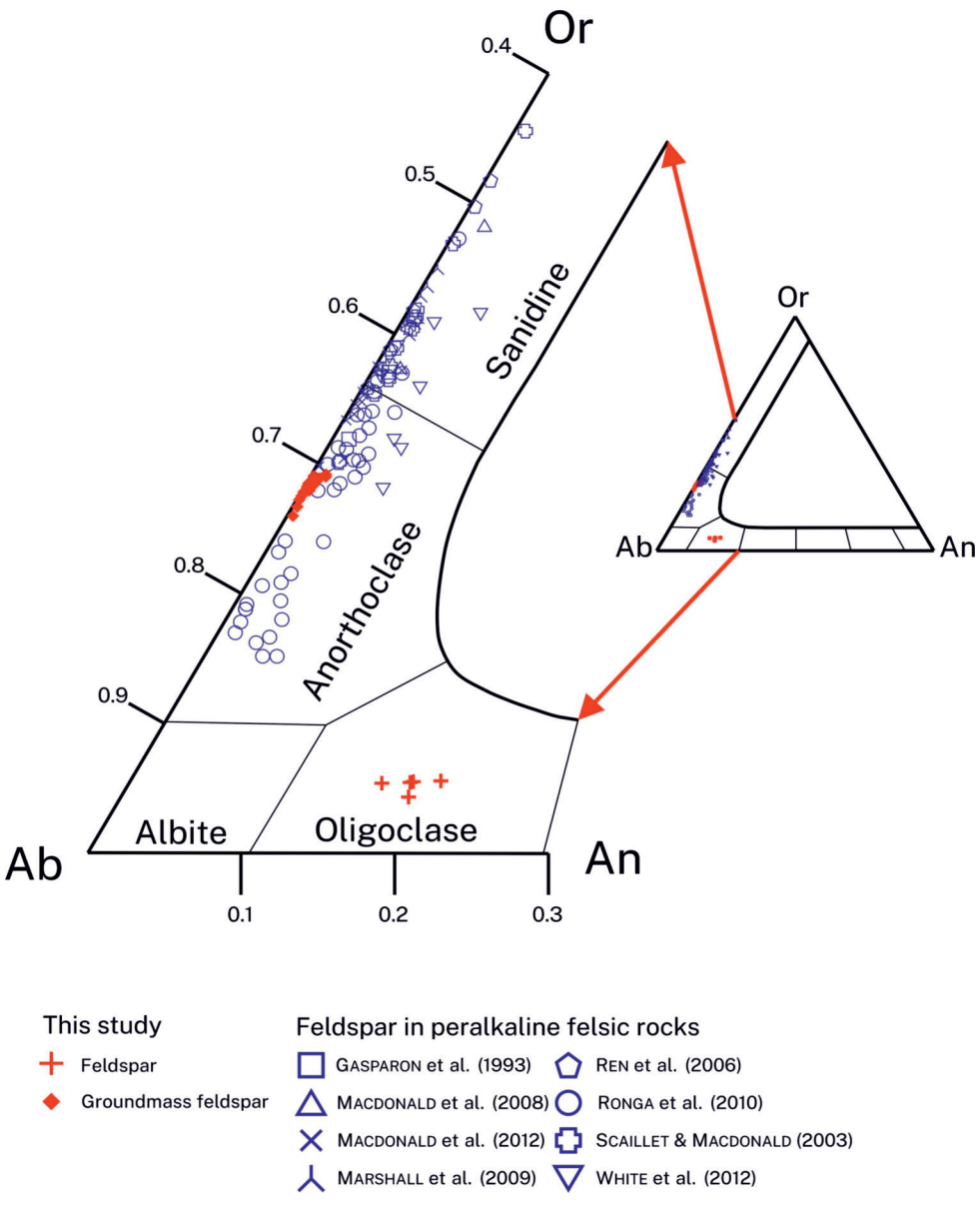

Figure 4. Ternary diagram showing the compositions (in mol%) for the studied feldspars from Oldoinyo Lengai compared to feldspars from peralkaline felsic rocks from the East African Rift System. Red – this study. Blue – feldspars in peralkaline silicic rocks from basalt-peralkaline silicic complexes at the East African Rift System. Classification diagram after Deer et al. (1992). Or – orthoclase ($KAlSi_3O_8$), Ab – albite ($NaAlSi_3O_8$), An – anorthite ($CaAl_2Si_2O_8$)

4. ábra. *Háromszögdiagram, amely a vizsgált Oldoinyo Lengai földpátok összetételét (mol%-ban) mutatja összehasonlítva a Kelet-afrikai-árokrendszerből származó más földpátokkal. Piros - jelen tanulmány. Kék - földpátok peralkáli szilikát kőzetekben a Kelet-afrikai-árokrendszer bazalt-peralkáli szilikát komplexumaiból. Osztályozás Deer et al. (1992) nyomán. Or - ortoklász ($KAlSi_3O_8$), Ab - albit ($NaAlSi_3O_8$), An - anortit ($CaAl_2Si_2O_8$)*

oligoclase feldspar cannot be formed by Oldoinyo Lengai silica-undersaturated alkali-rich magmatism. Quartz has been found in carbonatite-related REE deposits as inclusions in fluorite or coexisting with fluorite, leading to studies proposing that quartz may precipitate in carbonatite systems due to silicon fluoride species in hydrothermal processes (Huang et al. 2023). However, that mechanism does not seem to have played a role in our sample as no fluorite was found and no fluorine species were present in the quartz-hosted secondary fluid inclusions (Mororó et al. 2024). Quartz (*Fig. 4*) is also incompatible with the strong silica-undersaturated nature of Oldoinyo Lengai magmas (Klaudius & Keller 2006, Berkesi et al. 2020). Moreover, quartz and oligoclase feldspar show oriented appearance in the rock sample (*Fig. 3B*). As rutile needles were found in quartz, $aTiO_2$ was considered equal to 1 and temperatures were calculated by titanium-in-quartz geothermometry (Wark & Watson 2006). The calculated temperatures ranging from 473 °C to 526 °C (*Table III*) are not compatible with magmatic environments, suggesting metamorphic conditions. All the above points strongly support that quartz and oligoclase feldspar have a metamorphic origin and were preserved in the studied sample as relict crystals.

Table I. Representative compositions (in wt%) of the studied phases from the studied samples of Oldoinyo Lengai. FeOT – all Fe as FeO, fsp – feldspar, g-fsp – groundmass feldspar, cpx – clinopyroxene, ttn – titanite, gl – glass, MI – melt inclusion, sd – standard deviation, BD – below detection

I. táblázat. *Az Oldoinyo Lengairól származó minták vizsgált ásványainak reprezentatív összetétele (tömeg%). FeOT – az összes vas FeO-ban megadva, fsp – földpát, g-fsp – alapanyag földpát, cpx – klinopiroxén, ttn – titanit, gl – kőzetüveg, MI – olvadékzárvány, sd – szórás, BD – kimutatási határ alatti elem*

	fsp	sd	g-fsp	sd	cpx	sd	ttn	sd	gl	sd	MI	sd	Original Melt
SiO_2	62.3	0.4	67.1	0.4	51.5	0.4	32.5	0.4	73.3	0.4	66.0	0.6	58.2
TiO_2	-	-	-	-	1.1	0.1	39.3	0.5	0.8	0.1	2.6	0.2	2.7
Al_2O_3	23.6	0.2	18.6	0.2	0.7	0.1	0.2	0.1	7.4	0.2	7.2	0.2	7.5
FeO^T	BD	0.1	1.3	0.2	23.8	0.4	0.5	0.2	5.0	0.2	6.8	0.3	12.3
MnO	-	-	-	-	BD	0.1	BD	0.1	0.3	0.1	0.3	0.1	0.1
MgO	BD	0.1	BD	0.1	3.7	0.1	-	-	BD	0.1	0.7	0.1	1.6
SrO	BD	0.3	BD	0.3	-	-	BD	0.3	BD	0.4	0.4	0.4	-
CaO	4.3	0.1	BD	0.1	9.5	0.1	26.0	0.3	0.9	0.1	1.2	0.1	3.4
BaO	BD	0.2	BD	0.2	-	-	-	-	BD	0.3	BD	0.3	-
Na_2O	8.8	0.1	8.3	0.1	7.9	0.2	1.0	0.1	7.8	0.2	8.9	0.2	8.4
K_2O	0.9	0.1	4.6	0.1	-	-	-	-	4.4	0.1	5.2	0.1	5.6
P_2O_5	-	-	-	-	-	-	-	-	BD	0.1	0.3	0.1	-
Nb_2O_5	-	-	-	-	-	-	BD	0.2	-	-	-	-	-
SO_3	-	-	-	-	-	-	-	-	BD	0.1	BD	0.1	-
Sum	99.9		99.9		98.2		99.5		99.9		99.6		100.0

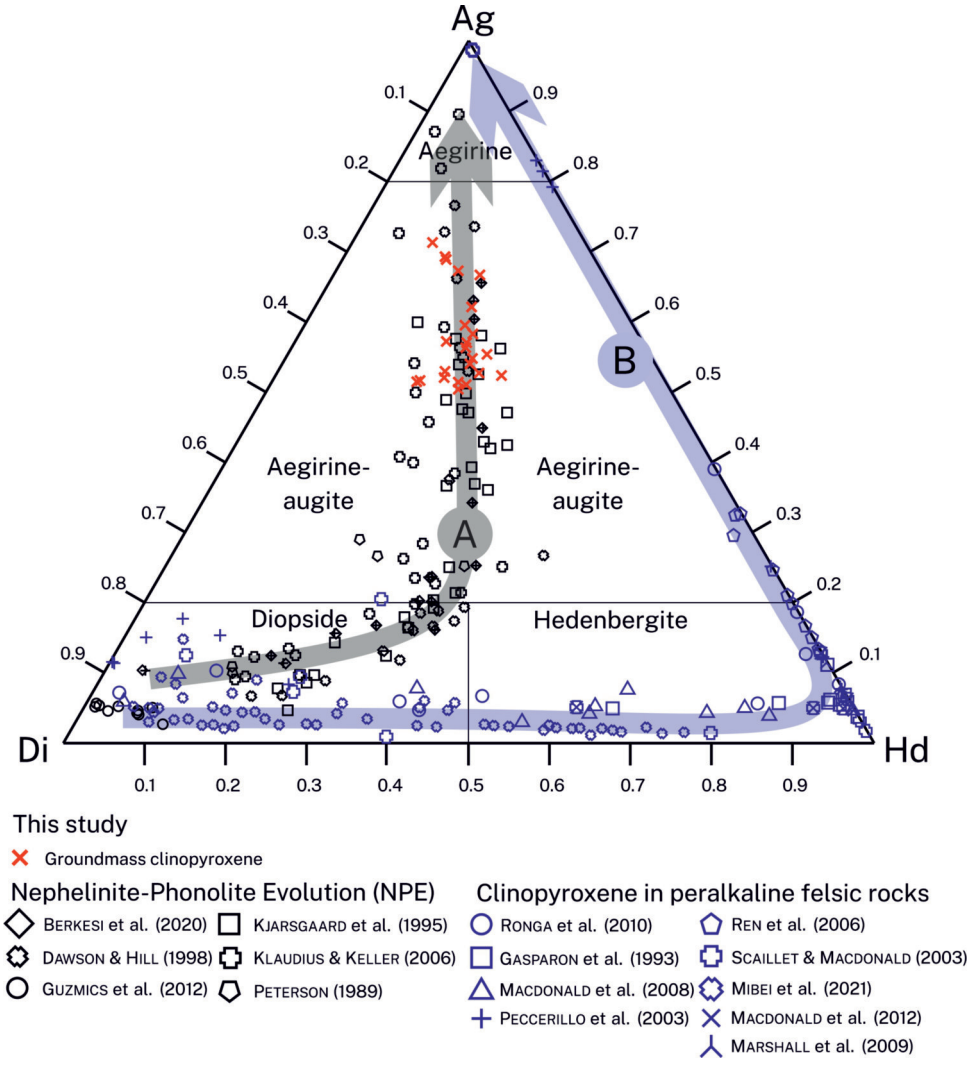

Figure 5. Compositions (in mol%) for the studied clinopyroxenes from Oldoinyo Lengai compared to clinopyroxenes from the East African Rift System. Aegirine-hedenbergite-diopside series classification diagram after MORIMOTO (1988)

Red – this study. Black – Clinopyroxene from Nephelinite-Phonolite Evolution (NPE). Blue – Clinopyroxenes from Basalt-Rhyolite Evolution (BRE). Ae – Aegirine, Hd – hedenbergite, Di – diopside

5. ábra. *A vizsgált Oldoinyo Lengai-ról származó klinopiroxének összetétele (mol%) összehasonlítva a Kelet-afrikai-árokrendszerből származó más klinopiroxénekkel. Egirin-hedenbergit-diopszid sorozat osztályozása MORIMOTO (1988) nyomán*

Piros – jelen tanulmány. Fekete – Klinopyroxén összetételek a nefelinit-fonolit fejlődési ágon (NPE). Kék – Klinopiroxének a bazalt-riolit fejlődési ágon (BRE). Ae – Egirin, Hd – hedenbergit, Di – diopszid

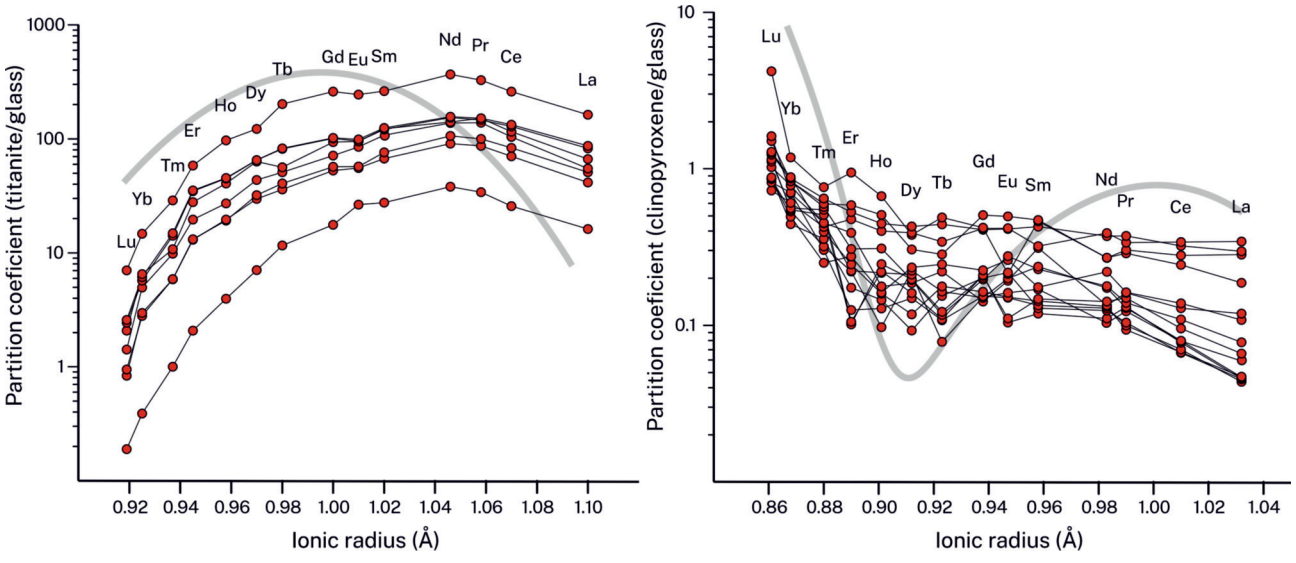

Figure 6. Onuma diagram (log solid / peralkaline rhyolitic glass partition coefficient vs. ionic radius) for titanite (left) and clinopyroxene (right) from xenolith samples collected at Oldoinyo Lengai. Compositions were determined by LA-ICP-MS. Light grey curves – theoretical partition coefficients between titanite/silicate melts (Prowatke & Klemme 2005) and aegirine/alkaline melts (Beard et al. 2019)

6. ábra. *Az Oldoinyo Lengai-on gyűjtött mintákból származó titanit (bal) és klinopiroxén (jobb) Onuma-diagramja. Az összetételt LA-ICP-MS módszerrel határoztuk meg. Világosszürke görbék – elméleti megoszlási együtthatók a titanit/szilikát olvadék (Prowatke & Klemme 2005) és az egirin/alkáli olvadék között (Beard et al. 2019)*

	Glass			Titanite		
	29d07	**29d39**	**29d41**	**29d04**	**29d22**	**29d44**
Li	10.1	10.4	8.6	<0.2	1.2	0.9
Cs	0.9	0.8	0.7	<0.1	0.1	<0.1
Rb	160.9	174.8	134.9	0.6	9.1	1.1
Th	12.9	6.7	4.3	0.3	3.0	4.0
U	4.4	1.9	1.4	0.8	8.9	10.4
Nb	54.5	35.2	28.2	2514.1	4396.4	6190.7
Ta	2.2	1.1	0.9	145.6	183.1	287.2
La	15.2	9.5	6.8	246.0	632.0	707.5
Ce	33.2	21.3	17.0	853.5	2462.1	2606.3
Pb	18.6	12.9	11.3	2.8	2.6	1.9
Pr	3.9	2.6	2.1	131.5	391.2	412.5
Sr	186.7	218.0	175.8	3121.3	1975.7	1862.6
Nd	14.1	10.5	8.5	535.9	1484.4	1620.1
Zr	947.9	338.8	229.1	151.4	1151.0	949.4
Hf	24.8	9.3	6.8	5.9	29.0	24.4
Sm	2.8	1.7	1.2	76.9	211.5	240.1
Eu	0.6	0.5	0.4	16.7	43.2	52.3
Gd	2.2	1.3	1.3	38.5	118.8	137.0
Ti	6098.7	6478.0	4344.8	234419.5	227382.9	242301.8
Tb	0.3	0.3	0.2	4.0	14.6	16.7
Dy	2.4	1.2	1.0	17.2	78.8	92.1
Y	13.9	8.5	5.0	31.0	211.3	243.1
Ho	0.5	0.3	0.2	1.8	11.5	13.0
Er	1.6	0.8	0.6	3.3	22.8	26.7
Tm	0.2	0.2	0.1	0.2	1.8	1.9
Yb	2.0	0.9	0.6	0.8	6.1	6.8
Lu	0.3	0.2	0.1	0.1	0.4	0.5
Zn	96.2	84.6	66.8	4.4	8.2	7.9
W	3.3	0.7	0.6	0.2	0.6	0.9
Mo	6.6	1.3	1.5	3.7	4.2	3.5
Sc	5.3	4.9	3.8	1.2	2.2	2.1
V	104.9	105.7	92.1	71.4	62.0	62.7

Table II. Representative trace element composition (in ppm) of the studied peralkaline rhyolite glass and titanite from Oldoinyo Lengai

II. táblázat. *Az Oldoinyo Lengai-ról származó, vizsgált peralkáli riolitos kőzetüveg és titanit reprezentatív nyom-elem-összetétele (ppm)*

Table III. Results of the titanium-in-quartz geothermometry. Titanium content (in ppm) of the studied relict quartz containing rutile inclusion and their calculated temperatures after WARK & WATSON (2006)

III. táblázat. *Titán a kvarcban geotermometria eredményei. A vizsgált, rutil kristályzárványt tartalmazó relikt kvarc titántartalma (ppm-ben) és kapott hőmérsékletei* WARK & WATSON *(2006) alapján*

Quartz	Ti (ppm)	T (°C)	Quartz	Ti (ppm)	T (°C)
1	9.8	509	**17**	10.5	514
2	10.1	511	**18**	10.5	514
3	10.3	513	**19**	10.4	514
4	10.8	516	**20**	8.1	496
5	7.6	491	**21**	10.0	510
6	7.1	486	**22**	8.3	497
7	7.6	491	**23**	11.4	520
8	9.1	504	**24**	6.0	476
9	10.1	511	**25**	8.2	496
10	7.3	488	**26**	7.8	493
11	11.4	520	**27**	7.5	490
12	7.3	489	**28**	14.0	536
13	11.4	520	**29**	12.1	525
14	6.9	485	**30**	12.4	526
15	13.4	532	**31**	12.0	524
16	10.6	515	**32**	5.8	473

Groundmass crystals

To understand the origin of groundmass crystals we compared our clinopyroxene composition to clinopyroxenes from magmatic systems that can produce aegirine-augite (*Fig. 5*). In a typical basalt-rhyolite evolution (*Fig. 5B*), primitive melts are Mg-rich crystallizing diopside (PECCERILLO et al. 2003, MACDONALD et al. 2008). They evolve towards Fe^{2+}-enriched compositions, precipitating hedenbergite (REN et al. 2006, RONGA et al. 2010). Fractional crystallization can eventually lead to peralkaline rhyolites with aegirine on a basalt-rhyolite evolutionary path (PECCERILLO et al. 2003, SCAILLET & MACDONALD 2003). Figure 5 shows compositional changes of clinopyroxene in a nephelinite-phonolite evolutionary path from Mg-rich diopside (GUZMICS et al. 2012), evolving towards Fe^{3+}-bearing diopside and to alkali-rich aegirine/aegirine-augite compositions (KJARSGAARD et al. 1995, KLAUDIUS & KELLER 2006), without precipitating Fe^{2+}-rich hedenbergite. Thus, our clinopyroxene composition cannot be a part of basalt-rhyolite evolution, owing to the lack of hedenbergite in our sample, at Oldoinyo Lengai (YAXLEY et al. 2022), and alkaline rocks in general. Both the aegirine-rich clinopyroxene (*Figs 3E, 5*) and the anorthoclase groundmass feldspar (*Figs 3C, 4*) indicate an alkali-rich magmatic origin, most likely associated with the Oldoinyo Lengai magmatism.

Peralkaline rhyolite glass

As shown above, groundmass crystals and relict crystals are coexisting but not coeval. This is supported by the abundance of fluid inclusions within relict crystals (*Fig. 3D*), and their absence in the groundmass (*Fig. 3E*). Peralkaline rhyolitic glass coexisting with euhedral clinopyroxene and groundmass feldspar (*Fig. 3E*) indicates an infiltration of a melt into a metamorphic rock (preserved as relict crystals), while the dissolved grain boundaries of the relict quartz and oligoclase feldspar (*Fig. 3C*) indicate the interaction of an infiltrating melt and a metamorphic rock (dissolution and assimilation). It should be noted that an in-situ partial melting of relict crystals could not form peralkaline compositions, as quartz does not contain alkalis and the relict oligoclase feldspar peralkalinity is less than 1 (*Table I, Supplementary Table I*).

Onuma diagrams (i.e., log solid/liquid partition coefficient vs. ionic radius) indicate that the groundmass clinopyroxene and peralkaline rhyolitic glass were not in equilibrium (*Fig. 6*), as curves near optimum radius are not parabolic (PHILPOTTS 1978, BLUNDY & WOOD 1994). The interaction of metamorphic rocks with Oldoinyo Lengai magmas must have happened shortly before eruption, preserving relict crystals, preventing groundmass crystals to reach equilibrium with the original melt, and preserving the melt as glass.

When considering silica-undersaturated magmatism, nepheline and perovskite are expected to crystalize instead of feldspar and titanite (BARKER 2001). The presence of groundmass feldspar and titanite, associated with dissolution features in quartz and replacement textures in oligoclase feldspar, indicate that the assimilation of a silica-rich metamorphic rock may have increased the silica activity of an initially silica-undersaturated melt. To estimate the original melt composition before assimilation a mass balance calculation was done. Firstly, titanite, clinopyroxene, and groundmass feldspar (*Table I, Supplementary Tables I-III*), based on their modal proportions, were added to the peralkaline rhyolite glass. Secondly, the relict crystal (quartz + relict oligoclase feldspar) modal proportion was removed from the combined groundmass composition (peralkaline rhyolite glass + titanite + clinopyroxene + groundmass feldspar), until one of the limiting parameters was reached ($Al_2O_3 > 8$ wt%, $TiO_2 > 3$ wt%, $FeO^T > 13$ wt%, peralkalinity index > 4). Constraints for realistic values for Al, Ti, Fe, and peralkaline index were set based on melt inclusion data from alkaline-silicate carbonatite systems (GUZMICS et al. 2012, 2015; BERKESI et al. 2023). Our calculation resulted in a peralkaline (peralkaline index = 2.66) phonolitic composition (*Fig. 7, Supplementary Table V*) for the original infiltrating melt. Nephelinitic compositions could not have been reached without FeO^T content and the peralkalinity index was unrealistic (> 15 wt% and > 4, respectively); thus, this composition was excluded. Therefore, the peralkalinity of the rhyolite glass (*Fig. 7, Supplementary Table IV*) can only have been inherited from the original melt (*Fig. 7,*

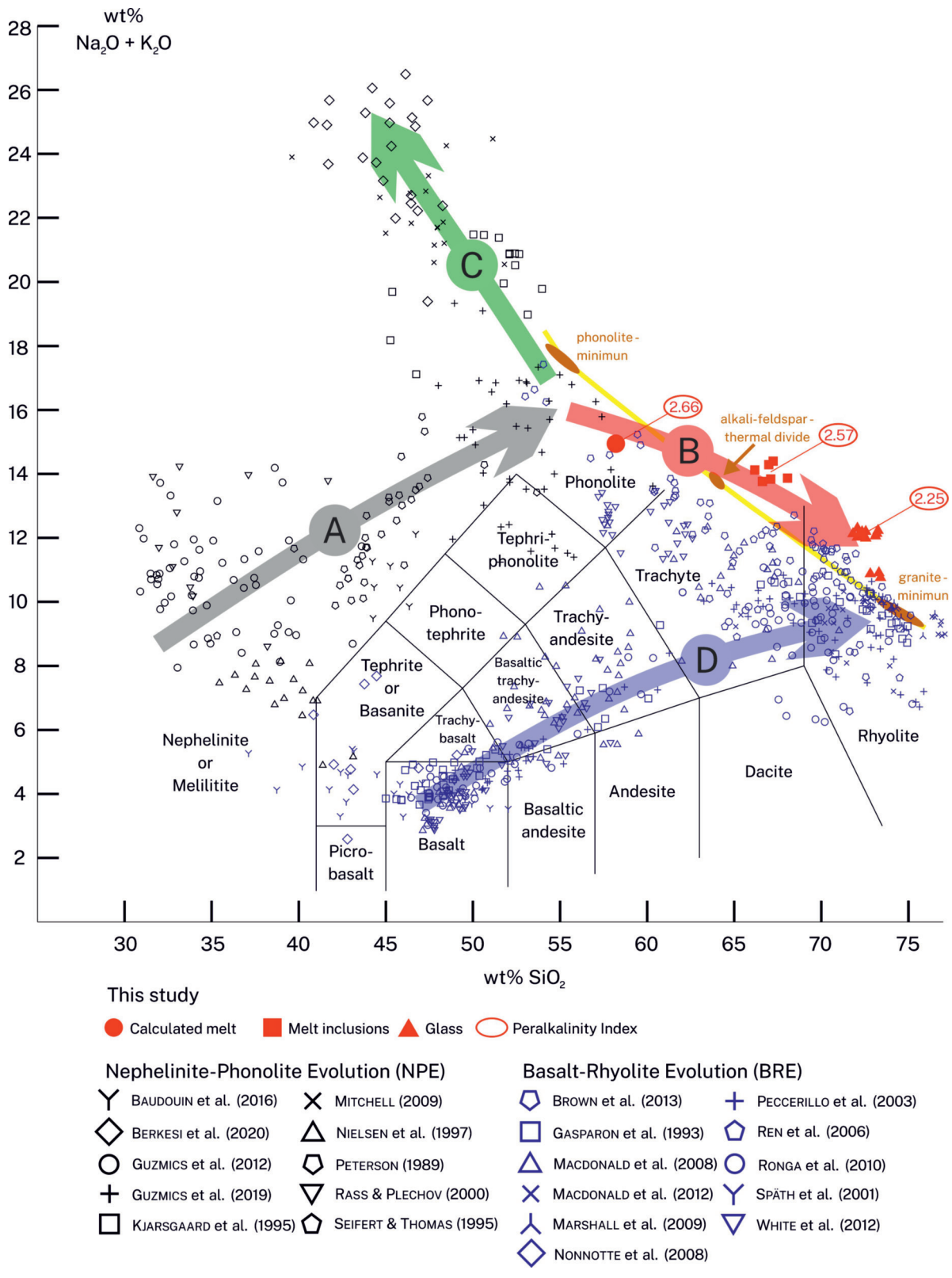

Figure 7. Total Alkali Silica (TAS) classification diagram after Maitre (2002). Orange – alkali-fedspar thermal divide after Schmidt & Weidendorfer (2018). A (grey arrow) – Nephelinite-Phonolite Evolution (NPE) trend, B (red arrow) – This study, an initially silica-undersaturated melt composition crosses the alkali-feldspar thermal divide by assimilating silica-rich rocks (i.e., metamorphic xenolith interacted with a melt belonging to the nephelinite-phonolite melt evolution), C (green arrow) – Re-equilibration of silicate melt and degassed fluid (Berkesi et al. 2020), D (blue arrow) – Basalt-Rhyolite Evolution (BRE) trend

7. ábra. *Teljes alkáli szilícium-dioxid (TAS) diagram Maitre (2002) nyomán. Narancssárga – alkáli földpát termikus gát Schmidt és Weidendorfer (2018) nyomán. A (szürke nyíl) – Nefelinit-fonolit fejlődés (NPE)., B (piros nyíl) – Jelen tanulmány. Egy kezdetben SiO_2-telítetlen olvadékösszetétel a szilícium-dioxidban gazdag kőzetek asszimilálásával átlépi az alkáli-földpát termikus gátat., C (zöld nyíl) – Szilikátolvadék és kigázosodott fluidum újra egyensúlyba jutása (Berkesi et al. 2020), D (kék nyíl) – Bazalt-riolit fejlődési trend (BRE).*

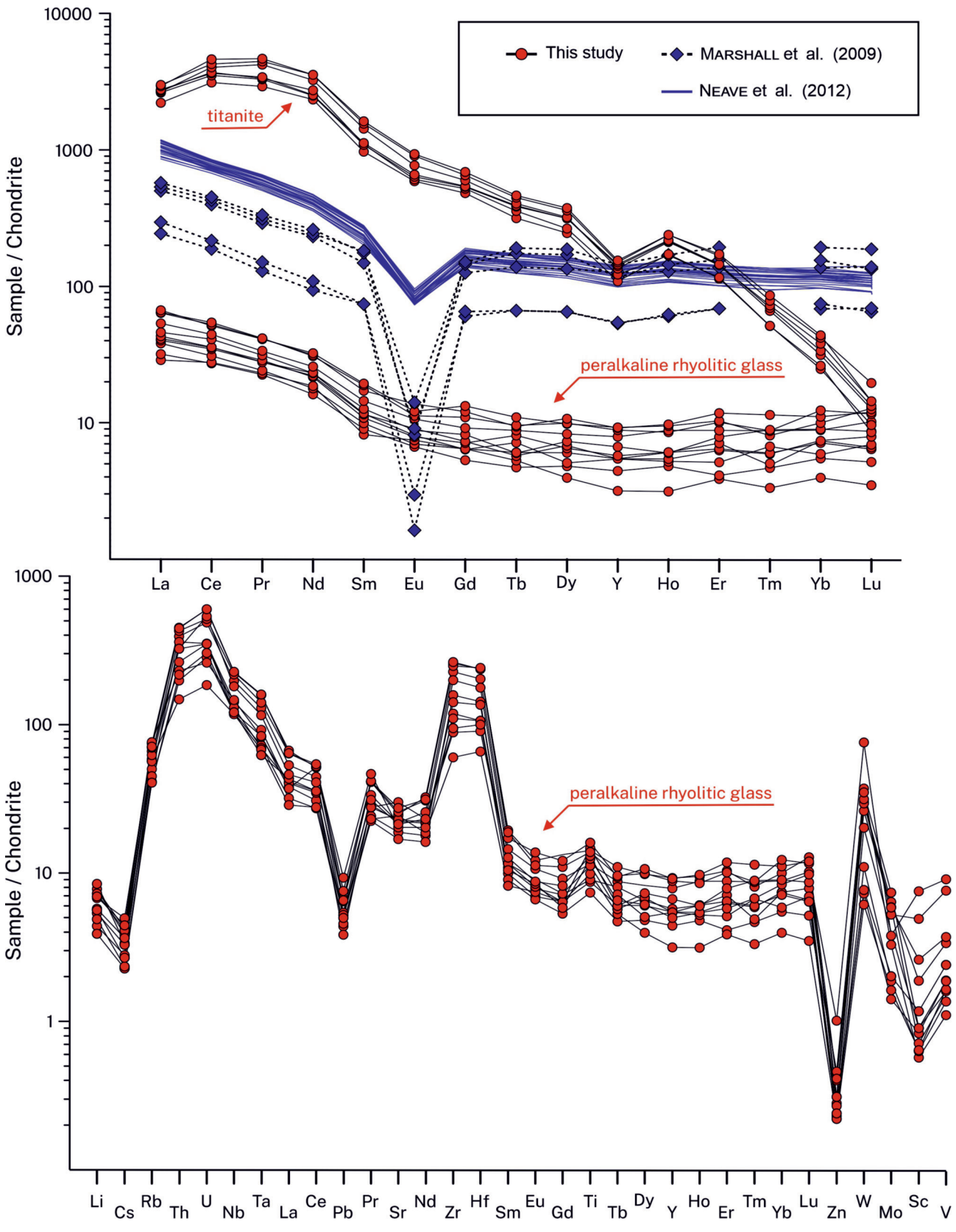

Figure 8. Chondrite-normalized (SUN & MCDONOUGH 1989) REE distributions of the studied peralkaline rhyolitic glass and titanite. Compositions were determined by LA-ICP-MS. Red – peralkaline rhyolitic glass and titanite from Oldoinyo Lengai (this study), blue diamond – peralkaline rhyolitic glass from Olkaria volcanic complex (MARSHALL et al. 2009), blue line – peralkaline rhyolitic glass from Pantelleria island (NEAVE et al. 2012)

8. ábra. *Kondritra normált (SUN & MCDONOUGH 1989) ritkaföldfém-eloszlás a vizsgált peralkáli riolitos üvegen és a titaniton. Az összetételeket LA-ICP-MS módszerrel határoztuk meg. Piros – peralkáli riolitos üveg és titanit Oldoinyo Lengai-ról (jelen tanulmány), kék gyémánt – peralkáli riolitos üveg az Olkaria vulkáni komplexumból (MARSHALL et al. 2009), kék vonal – peralkáli riolitos üveg Pantelleria szigetéről (NEAVE et al. 2012)*

Supplementary Table V), as partial melting of the relict crystals cannot contribute to increase in peralkalinity. Melt inclusions and rhyolite glass have lower peralkalinity than the original melt (*Fig. 7, Supplementary Tables IV-V*). This can be explained by the precipitation of aegirine, which is Na-rich and Al-poor (*Table I, Supplementary Table II*).

Assimilation vs. fractional crystallization

The fractionation of olivine, pyroxene, and plagioclase in dry, reduced, mantle plume/large igneous province-type rhyolites occurring in rift systems may result in elevated REE concentrations together with a negative Eu-anomaly (Jowitt et al. 2017). This is true for the EARS, where erupted rocks invariably have reduced oxygen fugacity (Biggs et al. 2021). Rocks from the Olkaria volcanic complex, located in the Gregory Rift (*Fig. 1*), also record an environment with reduced oxygen fugacity. Peralkaline rhyolite glass from the Olkaria volcanic complex presents negative Eu anomaly (Marshall et al. 2009), similar to the type locality for highly peralkaline rhyolites (i.e., pantellerites; Neave et al. 2012). Therefore, although the studied sample does not allow to infer redox conditions, the regional trend points towards an environment with reduced oxygen fugacity (Marshall et al. 2009, Biggs et al. 2021). Accordingly, the absence of negative Eu anomaly (*Fig. 8*) strongly suggests that peralkaline rhyolitic compositions at Oldoinyo Lengai were not formed by fractional crystallization as a typical basalt-rhyolite evolution.

Undoubtedly, peralkaline rhyolites and granites can be formed through fractional crystallization of initially basaltic/basanitic melts (Trua et al. 1999, Peccerillo et al. 2003, Macdonald et al. 2015). However, melts at Oldoinyo Lengai generally follow a nephelinite-phonolite evolution (Klaudius & Keller 2006; Berkesi et al. 2020, indicated by the grey arrow in *Fig. 7*). Enrichment of nephelinite melts in alkalis through re-equilibration with alkali carbonate fluid residues can generate highly peralkaline nephelinite melts (Berkesi et al. 2020; *Fig. 7*) but it is unlikely that such a melt would cross the alkali-feldspar thermal divide (Schmidt & Weidendorfer 2018) into rhyolitic compositions by crystal fractionation (*Fig. 7*). However, a phonolite melt (similar in composition to our estimated melt, *Fig. 7, Table I, Supplementary Table V*) can cross the alkali-feldspar thermal divide by assimilating silica-rich metamorphic rocks that are present in the surroundings of Oldoinyo Lengai (Smith & Mosley 1993, Macdonald et al. 2001).

Formation of peralkaline rhyolites through assimilation is not limited to Oldoinyo Lengai, similar processes have been proposed to explain the formation of peralkaline rhyolites in the Olkaria volcanic complex (Black et al. 1997).

Conclusions

The presence of anorthite and quartz is incompatible with Oldoinyo Lengai magmatism. The slight orientation of relict crystals, their silica-rich composition, and low formation temperatures (<530 °C) imply metamorphic origin. The alkali-rich groundmass minerals (aegirine, titanite) not being in equilibrium with the peralkaline rhyolite glass indicate that a metamorphic xenolith interacted with Oldoinyo Lengai alkali-rich magmatism shortly before eruption. The original melt composition was calculated as phonolitic (58.2 wt% SiO_2, 2.66 peralkalinity index). The absence of negative Eu anomaly rejects the possibility that these peralkaline rhyolite compositions could have been formed by fractional crystallization of a basalt melt. Combining the results on rhyolite glass, melt inclusion, and estimated original melt data, the assimilation of a silica-rich rock into a peralkaline silica-undersaturated melt can lead to compositions that cross the alkali-feldspar thermal divide and generate peralkaline rhyolite compositions (>66 wt% SiO_2, >2.2 peralkalinity index). The formation of peralkaline rhyolites through assimilation can occur in any continental rift where silica-undersaturated alkaline magmatism interacts with silica-rich country rocks. Such process may have been overlooked in other rift systems.

Acknowledgements

This manuscript is dedicated to the eminent career of Csaba Szabó, former supervisor of two authors of this paper (M. Berkesi and T. Guzmics). His support for the professional careers of M. Berkesi, T. Guzmics and E. Mororó is greatly acknowledged. Reviewers Enikő Bali and Milan Kohút provided very helpful and constructive comments on a draft version of this paper. M. Berkesi was supported by the fund of MTA-EPSS FluidsByDepth Research Group (LP2022-2/2022) and the NKFIH_FK132418 research grant. T. Guzmics was awarded the NKFIH_K142855 research grant.

References – Irodalom

Baudouin, C., Parat, F., Denis, C. M. M. & Mangasini, F. 2016: Nephelinite lavas at early stage of rift initiation (Hanang volcano, North Tanzanian Divergence). – *Contributions to Mineralogy and Petrology* **171,** 1–20. https://doi.org/10.1007/s00410-016-1273-5

Barker, D. S. 2001: Calculated silica activities in carbonatite liquids. – *Contributions to Mineralogy and Petrology* **141,** 704–709. https://doi.org/10.1007/s004100100281

Beard, C. D., van Hinsberg, V. J., Stix, J. & Wilke M. 2019: Clinopyroxene/Melt Trace Element Partitioning in Sodic Alkaline Magmas. – *Journal of Petrology* **60,** 1797–1824. https://doi.org/10.1093/petrology/egz052

Berkesi, M., Bali, E., Bodnar, R. J., Szabó, A. & Guzmics, T. 2020: Carbonatite and highly peralkaline nephelinite melts from Oldoinyo Lengai Volcano, Tanzania: The role of natrite-normative fluid degassing. – *Gondwana Research* **85,** 76–83. https://doi.org/10.1016/j.gr.2020.03.013

Berkesi, M., Myovela, J. L. & Guzmics, T. 2023: Carbonatite formation in continental settings via high pressure – high temperature liquid immiscibility. – *Geochimica et Cosmochimica Acta* **349,** 41–54. https://doi.org/10.1016/j.gca.2023.03.027

Biggs, J., Ayele, A., Fischer, T. P., Fontijn, K., Hutchison, W., Kazimoto, E., Whaler, K. & Wright, T. J. 2021: Volcanic activity and hazard in the East African Rift Zone. – *Nature Communications* **12,** 6881. https://doi.org/10.1038/s41467-021-27166-y

Black, S., Macdonald, R. & Kelly, M. R. 1997: Crustal Origin for Peralkaline Rhyolites from Kenya: Evidence from U-Series Disequilibria and Th-Isotopes. – *Journal of Petrology* **38,** 227–297. https://doi.org/10.1093/petroj/38.2.277

Blundy, J. & Wood, B. 1994: Prediction of crystal–melt partition coefficients from elastic moduli. – *Nature* **372,** 452–454. https://doi.org/10.1038/372452a0

Braile, L. W., Keller, G. R., Wendlandt, R. F., Morgan, P. & Khan, M. A. 2006: The East African rift system. – *Developments in Geotectonics* **25,** 213–231. https://doi.org/10.1016/S0419-0254(06)80013-3

Brown, F. H., Nash, B. P., Fernandez, D. P., Merrick, H. V. & Thomas, R. J. 2013: Geochemical composition of source obsidians from Kenya. – *Journal of Archaeological Science* **40,** 3233–3251. https://doi.org/10.1016/j.jas.2013.03.011

Bryan, S. E., Ferrari, L., Reiners, P. W., Allen, C. M., Petrone, C. M., Ramos-Rosique, A. & Campbell, I. H. 2008: New insights into crustal contributions to large-volume rhyolite generation in the mid-Tertiary Sierra Madre Occidental province, Mexico, revealed by U-Pb geochronology. – *Journal of Petrology* **49,** 47–77. https://doi.org/10.1093/petrology/egm070

Chorowicz, J. 2005: The East African rift system. – *Journal of African Earth Sciences* **42,** 379–410. https://doi.org/10.1016/j.jafrearsci.2005.07.019

Colby, D. J., Pyle, D. M., Fontijn, K., Mather, T. A., Melaku, A. A., Mengesha, M. A. & Yirgu, G. 2022: Stratigraphy and eruptive history of Corbetti Caldera in the Main Ethiopian Rift. – *Journal of Volcanology and Geothermal Research* **428,** 107580. https://doi.org/10.1016/j.jvolgeores.2022.107580

Dawson, J. B. 2008: *The Gregory Rift Valley and Neogene-Recent Volcanoes of Northern Tanzania. – Memoirs of the Geological Society of London* **33,** London. https://doi.org/10.1144/M33

Dawson, J. B. & Hill, P. G. 1998: Mineral chemistry of a peralkaline combeite-lamprophyllite nephelinite from Oldoinyo Lengai, Tanzania. – *Mineralogical Magazine* **62,** 179–196. https://doi.org/10.1180/002646198547567

Dawson, J. B., Smith, J. V. & Steele, I. M. 1992: 1966 ash eruption of the carbonatite volcano Oldoinyo Lengai: mineralogy of lapilli and mixing of silicate and carbonate magmas. – *Mineralogical Magazine* **56,** 1–16. https://doi.org/10.1180/minmag.1992.056.382.01

Deer, W. A., Howie, R. A. & Zussman, J. 1992: *An introduction to the Rock Forming Minerals, 2nd ed.* – Longman Group Ltd., Harlow, 712 pp. https://doi.org/10.1180/DHZ

Dostal, J. 2017: Rare Metal Deposits Associated with Alkaline/Peralkaline Igneous Rocks. – *Resources* **6,** 34. https://doi.org/10.3390/resources6030034

Fritz, H., Abdelsalam, M., Ali, K. A., Bingen, B., Collins, A. S., Fowler, A. R., Ghebreab, W., Hauzenberger, C. A., Johnson, P. R., Kusky, T. M., Macey, P., Muhongo, S., Stern, R. J. & Viola, G. 2013: Orogen styles in the East African Orogen: A review of the Neoproterozoic to Cambrian tectonic evolution. – *Journal of African Earth Sciences* **86,** 65–106. https://doi.org/10.1016/j.jafrearsci.2013.06.004

Gasparon, M., Innocenti, F., Manetti, P., Peccerillo, A. & Tsegaye, A. 1993: Genesis of the pliocene to recent bimodal mafic-felsic volcanism in the Debre Zeyt area, central Ethiopia: volcanological and geochemical constraints. – *Journal of African Earth Sciences (and the Middle East)* **17,** 145–165. https://doi.org/10.1016/0899-5362(93)90032-L

Guillong, M., Meier, D. L., Allan, M. M., Heinrich, C. A. & Yardley, B. W. D. 2008: SILLS: A MATLAB-based program for the reduction of laser ablation ICP–MS data of homogeneous materials and inclusions. – In: Sylvester, P.: *Laser Ablation–ICP–MS in the Earth Sciences – Current Practices* and *Outstanding Issues*. – Mineralogical Association of Canada Short Course Series Volume 40, Vancouver.

Guzmics, T., Mitchell, R. H., Szabó, C., Berkesi, M., Milke, R. & Ratter, K. 2012: Liquid immiscibility between silicate, carbonate and sulfide melts in melt inclusions hosted in co-precipitated minerals from Kerimasi volcano (Tanzania): Evolution of carbonated nephelinitic magma. – *Contributions to Mineralogy and Petrology* **164**, 101–122. https://doi.org/10.1007/s00410-012-0728-6

Guzmics, T., Zajacz, Z., Mitchell, R. H., Szabó, C. & Wälle, M. 2015: The role of liquid–liquid immiscibility and crystal fractionation in the genesis of carbonatite magmas: insights from Kerimasi melt inclusions. – *Contributions to Mineralogy and Petrology* **169,** 17. https://doi.org/10.1007/s00410-014-1093-4

Guzmics, T., Berkesi, M., Bodnar, R. J., Fall, A., Bali, E., Milke, R., Vetlényi, E. & Szabó, C. 2019: Natrocarbonatites: A hidden product of three-phase immiscibility. – *Geology* **47,** 527–530. https://doi.org/10.1130/G46125.1

Halder, M., Paul, D. & Sensarma S. 2021: Rhyolites in continental mafic Large Igneous Provinces: Petrology, geochemistry and petrogenesis. – *Geoscience Frontiers* **12,** 53–80. https://doi.org/10.1016/j.gsf.2020.06.011.

Halász, N., Berkesi, M., Tóth, T. M., Mitchell, R. H., Milke, R. & Guzmics, T. 2023: Reconstruction of magma chamber processes preserved in olivine-phlogopite micro-ijolites from the Oldoinyo Lengai, Tanzania. – *Journal of African Earth Sciences* **197,** 104738. https://doi.org/10.1016/j.jafrearsci.2022.104738.

Hay, D. E., Wendlandt, R. F. & Wendlandt, E. D. 1995: The origin of Kenya rift plateau-type flood phonolites: evidence from geochemical studies for fusion of lower crust modified by alkali basaltic magmatism. – *Journal of Geophysical Research* **100,** 411–422. https://doi.org/10.1029/94JB02159

Huang, Y., Liu, Q., Liu, F., Li, X., Liu, Y., Tang, G., Fan, H., Li, X. & Li, Q. 2023: Large Si isotope fractionation reveals formation mechanism of quartz in silicon-poor carbonatite. – *Geology* **51,** 1038–1042. https://doi.org/10.1130/G51314.1

Hutchison, W., Pyle, D. M., Mather, T. A., Yirgu, G., Biggs, J., Cohen, B. E., Barfod, D. N. & Lewi, E. 2016: The eruptive history and magmatic evolution of Aluto volcano: new insights into silicic peralkaline volcanism in the Ethiopian rift. – *Journal of Volcanology and Geothermal Research* **328,** 9–33. https://doi.org/10.1016/j.jvolgeores.2016.09.010

Jowitt, S. M., Medlin, C. C. & Cas, R. A. F. 2017: The rare earth element (REE) mineralisation potential of highly fractionated rhyolites: A potential low-grade, bulk tonnage source of critical metals. – *Ore Geology Reviews* **86,** 548–562. https://doi.org/10.1016/j.oregeorev.2017.02.027

Jung, S., Hoernes, S. & Hoffer, E. 2005: Petrogenesis of Cogenetic Nepheline and Quartz Syenites and Granites (Northern Damara Orogen, Namibia): Enriched Mantle versus Crustal Contamination. – *Journal of Geology* **113,** 651–672. http://dx.doi.org/10.1086/467475

Káldos, R., Guzmics, T. Mitchell, R. H., Dawnson, J. B., Milke, R. & Szabó, C. 2015: A melt evolution model for Kerimasi volcano, Tanzania: Evidence from carbonate melt inclusions in jacupirangite. – *Lithos* **238,** 101–119. http://dx.doi.org/10.1016/j.lithos.2015.09.011

Kampunzu, A. B., Bonhomme, M. G. & Kanika, M. 1998: Geochronology of volcanic rocks and evolution of the Cenozoic western branch of the East African Rift system. – *Journal of African Earth Sciences* **26,** 441–461. https://doi.org/10.1016/S0899-5362(98)00025-6

Keller, G. R., Prodehl, C., Mechie, J., Fuchs, K., Khan, M. A., Maguire, P. K. H., Mooney, W. D., Achauer, U., Davis, P. M., Meyer, R. P., Braile, L. W., Nyambok, I. O. & Thompson, G. A. 1994: The East African rift system in the light of KRISP 90. – *Tectonophysics* **236,** 465–483. https://doi.org/10.1016/0040-1951(94)90190-2

Kjarsgaard, B. A., Hamilton, D. L. & Peterson, T. D. 1995: *Peralkaline Nephelinite/Carbonatite Liquid Immiscibility: Comparison of Phase Compositions in Experiments and Natural Lavas from Oldoinyo Lengai.* – In: Bell, K. & Keller, J. (eds): *Carbonatite Volcanism*, IAVCEI Proceedings in Volcanology, vol 4. Springer, Berlin, Heidelberg. https://doi.org/10.1007/978-3-642-79182-6_13

Klaudius, J. & Keller, J. 2006: Peralkaline silicate lavas at Oldoinyo Lengai, Tanzania. – *Lithos* **91,** 173–190. https://doi.org/10.1016/j.lithos.2006.03.017

Kracek, F. C., Bowen, N. L. & Morey, G. W. 1937: Equilibrium Relations and Factors Influencing Their Determination in the System K_2SiO_3–SiO_2. – *The Journal of Physical Chemistry* **41,** 1183–1193. https://doi:10.1021/j150387a004

LeMasurier, W. E., Futa, K., Hole, M. & Kawachi, Y. 2005: Polybaric Evolution of Phonolite, Trachyte, and Rhyolite Volcanoes in Eastern Marie Byrd Land, Antarctica: Controls on Peralkalinity and Silica Saturation. – *International Geology Review* **45,** 1055–1099. http://dx.doi.org/10.2747/0020-6814.45.12.1055

Lowenstern, J. B. & Mahood, G. A. 1991: New data on magmatic H_2O contents of pantellerites, with implications for petrogenesis and eruptive dynamics at Pantelleria. – *Bulletin of Volcanology* **54,** 78–83. https://doi.org/10.1007/bf00278208

McConnell, R. B. 1972: Geological Development of the Rift System of Eastern Africa. – *GSA Bulletin* **83,** 2549–2572. https://doi.org/10.1130/0016-7606(1972)83[2549:GDOTRS]2.0.CO;2

Macdonald, R. & Scaillet, B. 2006: The central Kenya peralkaline province: Insights into the evolution of peralkaline salic magmas. – *Lithos* **91,** 59–73. https://doi.org/10.1016/j.lithos.2006.03.009.

Macdonald, R. Davies, G. R., Bliss, C. M., Leat, P. T., Bailey, D. K. & Smith, R. L. 1987: Geochemistry of High-silica Peralkaline Rhyolites, Naivasha, Kenya Rift Valley. – *Journal of Petrology* **28,** 979–1008. https://doi.org/10.1093/petrology/28.6.979

Macdonald, R., Rogers, N. W., Fitton, J. G., Black, S. & Smith, M. 2001: Plume–Lithosphere Interactions in the Generation of the Basalts of the Kenya Rift, East Africa. – *Journal of Petrology* **42,** 877–900. https://doi.org/10.1093/petrology/42.5.877

Macdonald, R., Belkin, H. E., Fitton, J. G., Rogers, N. W., Nejbert, K., Tindle, A. G. & Marshall, A. S. 2008: The Roles of Fractional Crystallization, Magma Mixing, Crystal Mush Remobilization and Volatile–Melt Interactions in the Genesis of a Young Basalt–Peralkaline Rhyolite Suite, the Greater Olkaria Volcanic Complex, Kenya Rift Valley. – *Journal of Petrology* **49,** 1515–1547. https://doi.org/10.1016/j.oregeorev.2017.02.027

Macdonald, R., Baginski, B., Ronga, F., Dzierzanowski, P., Lustrino, M., Marzoli, A. & Melluso, L. 2012: Evidence for extreme fractionation of peralkaline silicic magmas, the Boseti volcanic complex, Main Ethiopian Rift. – *Mineralogy and Petrology* **104,** 163–175. https://doi.org/10.1007/s00710-011-0184-4

Macdonald, R., Sumita, M., Schmincke, H., Baginski, B., White, J. C. & Ilnicki, S. S. 2015: Peralkaline felsic magmatism at the Nemrut volcano, Turkey: impact of volcanism on the evolution of Lake Van (Anatolia) IV. – *Contributions to Mineralogy and Petrology* **169,** 34. https://doi.org/10.1007/s00410-015-1127-6

Marshall, A. S., Macdonald, R., Rogers, N. W., Fitton, J. G., Tindle, A. G., Nejbert, K. & White, R. W. 2009: Fractionation of Peralkaline Silicic Magmas: the Greater OlkariaVolcanic Complex, Kenya Rift Valley. – *Journal of Petrology* **50,** 323–359. https://doi.org/10.1093/petrology/egp001

Mibei, G., Bali, E., Geirsson, H., Guðfinnsson, G. H., Harðarson, B. S. & Franzson, H. 2021: Partial melt generation and evolution of magma reservoir conditions at the Paka volcanic complex in Kenya: Constraints from geochemistry, petrology and geophysics. – *Lithos* **400–401,** 106385. https://doi.org/10.1016/j.lithos.2021.106385

Mitchell, R. H. 2009: Peralkaline nephelinite–natrocarbonatite immiscibility and carbonatite assimilation at Oldoinyo Lengai, Tanzania. – *Contributions to Mineralogy and Petrology* **158,** 589–598. https://doi.org/10.1007/s00410-009-0398-1

Mooney, W. D. & Christensen, N. I. 1994: Composition of the crust beneath the Kenya rift. – *Tectonophysics* **236,** 391–408. https://doi.org/10.1016/0040-1951(94)90186-4

Morimoto, N. 1988: Nomenclature of Pyroxenes. – *Mineralogy and Petrology* **39,** 55–76. https://doi.org/10.1007/BF01226262

Mororó, E. A. A., Berkesi, M., Zajacz, Z. & Guzmics, T. 2024: Rare earth element transport and mineralization linked to fluids from carbonatite systems. – *Geology* **52/4,** 240–244. https://doi.org/10.1130/G51531.1

Muhongo, S. 1999: Anatomy of the Mozambique Belt of Eastern and Southern Africa: Evidence from Tanzania. – *Gondwana Research* **2,** 369–375. https://doi.org/10.1016/S1342-937X(05)70276-8

Neave, D. A., Fabbro, G., Herd, R. A., Petrone, C. M. & Edmonds, M. 2012: Differentiation and Degassing at the Pantelleria Volcano. – *Journal of Petrology* **53,** 637–663. https://doi.org/10.1093/petrology/egr074

Nielsen, T. F. D., Solovova, I. P. & Veksler, I. V. 1997: Parental melts of melilitolite and origin of alkaline carbonatite: evidence from crystallised melt inclusions, Gardiner complex. – *Contributions to Mineralogy and Petrology* **126,** 331–344.

Nonnotte, P., Benoit, M., Le Gall, B., Hémond, C., Rolet, J., Cotten, J., Brunet, P. & Makoba, E. 2011: Petrology and geochemistry of alkaline lava series, Kilimanjaro, Tanzania: New constraints on petrogenetic processes. – *The Geological Society of America, Special Paper* **478,** 127–158. https://doi.org/10.1130/2011.2478(07)

Peccerillo, A., Barberio, M. R., Yirgu, G., Ayalew, D., Barbieri, M. & Wu, T. W. 2003: Relationships between Mafic and Peralkaline Silicic Magmatism in Continental Rift Settings: a Petrological, Geochemical and Isotopic Study of the Gedemsa Volcano, Central Ethiopian Rift. – *Journal of Petrology* **44,** 2003–2032. https://doi.org/10.1093/petrology/egg068

Peterson, T. D. 1989: Peralkaline nephelinites. I. Comparative petrology of Shombole and Oldoinyo L'engai, East Africa. – *Contributions to Mineralogy and Petrology* **101,** 458–478. https://doi.org/10.1007/BF00372219

Philpotts, J. A. 1978: The law of constant rejection. – *Geochimica et Cosmochimica Acta* **42,** 909–920. https://doi.org/10.1016/0016-7037(78)90102-3

Prodehl, C., Jacob, A. W. B., Thybo, H., Dindi, E. & Stangl, R. 1994: Crustal structure on the northeastern flank of the Kenya rift. – *Tectonophysics* **236,** 271–290. https://doi.org/10.1016/0040-1951(94)90180-5

Prowatke, S. & Klemme, S. 2005: Effect of melt composition on the partitioning of trace elements between titanite and silicate melt. – *Geochimica et Cosmochimica Acta* **69,** 695–709. https://doi.org/10.1016/j.gca.2004.06.037

Rass, I. T. & Plechov, P. Y. 2000: Melt inclusions in olivines from the olivine-melilitite rock of the Guli massif, northwestern Siberian platform. – *Doklady Earth Sciences* **375A,** 1399–1402.

Ren, M., Omenda, P. A., Anthony, E. Y., White, J. C., Macdonald, R. & Bailey, D. K. 2006: Application of the QUILF thermobarometer to the peralkaline trachytes and pantellerites of the Eburru volcanic complex, East African Rift, Kenya. – *Lithos* **91,** 109–124. https://doi.org/10.1016/j.lithos.2006.03.011

Ronga, F., Lustrino, M., Marzoli, A. & Melluso, L. 2010: Petrogenesis of a basalt-comendite-pantellerite rock suite: the Boseti Volcanic Complex (Main Ethiopian Rift). – *Mineralogy and Petrology* **98,** 227–243. https://doi.org/10.1007/s00710-009-0064-3

Rosendahl, B. R. 1987: Architecture of Continental Rifts with Special Reference to East Africa. – *Annual Reviews* **15,** 445–503. https://doi.org/10.1146/annurev.ea.15.050187.002305

Scaillet, B. & Macdonald, R. 2003: Experimental Constraints on the Relationships between Peralkaline Rhyolites of the Kenya Rift Valley. – *Journal of Petrology* **44,** 1867–1894. https://doi.org/10.1093/petrology/egg062

Scaillet, B. & Macdonald, R. 2006: Experimental and Thermodynamic Constraints on the Sulphur Yield of Peralkaline and Metaluminous Silicic Flood Eruptions. – *Journal of Petrology* **47,** 1413–1437. https://doi.org/10.1093/petrology/egl016

Schmidt, M. W. & Weidendorfer, D. 2018: Carbonatites in oceanic hotspots. – *Geology* **46,** 435–438. https://doi.org/10.1130/G39621.1

Seifert, W. & Thomas, R. 1995: Silicate-carbonate immiscibility: A melt inclusion study of olivine melilitite and wehrlite xenoliths in Tephrite from the Elbe Zone, Germany. – *Chemie der Erde* **55,** 263–279.

Smith, M. & Mosley, P. 1993: Crustal heterogeneity and basement influence on the development of the Kenya Rift, East Africa. – *Tectonics* **12,** 591–605. https://doi.org/10.1029/92tc01710

Späth, A., Le Roex, A. P. & Opiyo-Akech, N. 2001: Plume–Lithosphere Interaction and the Origin of Continental Rift-related Alkaline Volcanism—the Chyulu Hills Volcanic Province, Southern Kenya. – *Journal of Petrology* **42,** 765–787. https://doi.org/10.1093/petrology/42.4.765

Sun, S.-s. & McDonough, W. F. 1989: Chemical and isotopic systematics of oceanic basalts: implications for mantle composition and processes. – *Geological Society London Special Publications* **42,** 313–345. https://doi.org/10.1144/GSL.SP.1989.042.01.19

Trua, T., Deniel, C. & Mazzuoli, R. 1999: Crustal control in the genesis of Plio-Quaternary bimodal magmatism of the Main Ethiopian Rift (MER): geochemical and isotopic (Sr, Nd, Pb) evidence. – *Chemical Geology* **155,** 201–231. https://doi.org/10.1016/S0009-2541(98)00174-0

Wang, Z., Fan, H., Zhou, L., Yang, K. & She, H. 2020: Carbonatite-Related REE Deposits: An Overview. – *Minerals* **10,** 965. https://doi.org/10.3390/min10110965

Wark, D. A. & Watson, E. B. 2006: TitaniQ: a titanium-in-quartz geothermometer. – *Contributions to Mineralogy and Petrology* **152,** 743–754. https://doi.org/10.1007/s00410-006-0132-1

White, J. C., Espejel-García, V. V., Anthony, E. Y. & Omenda, P. 2012: Open System evolution of peralkaline trachyte and phonolite from the Suswa volcano, Kenya rift. – *Lithos* **152,** 84–104. https://doi.org/10.1016/j.lithos.2012.01.023

Yaxley, G. M., Anenburg, M., Tappe, S., Decree, S. & Guzmics, T. 2022: Carbonatites: Classification, Sources, Evolution, and Emplacement. – *Annual Review of Earth and Planetary Sciences* **50,** 261–93. https://doi.org/10.1146/annurev-earth-032320-104243

Manuscript received: 20/03/2024

Digital supplementaries

Supplementary Table I. Composition (in wt%) of the studied feldspar from Oldoinyo Lengai, data from groundmass crystals and relicts (core & rim)
Melléklet I. táblázat. A vizsgált Oldoinyo Lengai-ról származó földpát összetétele (tömeg%) mind az alapanyag, mind a relikt földpát kristályokból (mag és perem)

Supplementary Table II. Composition (in wt%) of the studied clinopyroxene from Oldoinyo Lengai, data from groundmass crystals
Melléklet II. táblázat. Az Oldoinyo Lengai vizsgált klinopiroxének összetétele (tömeg%), adatok az alapanyag kristályokból

Supplementary Table III. Composition (in wt%) of the studied titanite from Oldoinyo Lengai, data from groundmass crystals (core & rim)
Melléklet III. táblázat. A vizsgált Oldoinyo Lengai-ról származó titanit összetétele (tömeg%) alapanyag kristályokból (mag és perem)

Supplementary Table IV. Composition (in wt%) of the studied glass from Oldoinyo Lengai
Melléklet IV. táblázat. A vizsgált Oldoinyo Lengai-ról származó kőzetüveg összetétele (tömeg%)

Supplementary Table V. Composition (in wt%) of the studied melt inclusions from Oldoinyo Lengai and the estimated original melt
Melléklet V. táblázat. A vizsgált Oldoinyo Lengai-ról származó olvadékzárványok és a becsült eredeti olvadék összetétele (tömeg%)

Supplementary Table VI. Trace element composition (in ppm) of the studied peralkaline rhyolite glass from Oldoinyo Lengai
Melléklet VI. táblázat. Oldoinyo Lengai-ról származó vizsgált peralkáli riolitüveg nyomelem-összetétele (ppm)

Supplementary Table VII. Trace element composition (in ppm) of the studied titanite from Oldoinyo Lengai
Melléklet VII. táblázat. A vizsgált Oldoinyo Lengai titanitok nyomelem-összetétele (ppm)